Simulation of the incompressible flow through a jet engine fuel nozzle rig

By X. Wu, G. Iaccarino, F. Ham AND P. Moin

1. Motivation and objectives

Swirling flow discharged from an injector nozzle is important for flame stabilization in the jet engine combustion process. Inclusion of the details of the swirl-generating device, i.e., the realistic injector nozzle geometry, in combustor numerical simulation is necessary because the complicated, spatially developing swirl pattern produced by a nozzle is difficult to emulate faithfully using indirect means. An indirect approach of swirl generation for large-eddy simulation was developed by Pierce & Moin (1998). Brankovic *et al.* (2000) reported comparison of laser velocimetry measurements with unstructured Reynolds-Averaged (RANS) predictions of incompressible swirling flow through a jet engine fuel nozzle rig. The actual hardware studied was a low-emission fuel nozzle and swirler combination, representative of current production engines. Their unstructured mesh has a total of 2.55 million hexahedral elements covering a 180° periodic sector of the injector, and was generated by simplifying a CAD model. The computations of Brankovic *et al.* were performed using the National Combustion Code (NCC). They found that quantitative accuracy was not achieved by the calculation. In particular, Brankovic *et al.* pointed out that the central recirculation zone measured from their own laser velocimetry experiments is both larger in extent, and has higher reverse flow than could be predicted using their computational approach. Other recent calculations of swirling flow in jet engine combustor with the full injector configuration were reported by Grinstein *et al.* (2002) and Roux *et al.* (2005).

Mahesh *et al.* (2004) developed an unstructured fractional-step algorithm for LES of incompressible flow in complex geometries. Their fractional-step method uses collocated grids and is formulated with combined usages of cell center based Cartesian velocity and face center based face normal velocity; pressure is stored at cell center. Discrete kinetic energy conservation is achieved by proper handling of the convection and pressure-gradient terms. Integrated global contribution of the convective term to discrete kinetic energy is zero if values at the face center are calculated as a simple arithmetic mean of the values at the two cell centers that have that particular face in common. Although pressure gradient term is globally non-conservative in the equation of discrete kinetic energy, its effect can be reduced through a least-square minimization procedure. Mahesh *et al.* applied their algorithm to the flow in one sector of a jet engine combustor. The predicted mass flow splits through various injector nozzle components compare very well with measurements. No detailed comparisons of the combustor flow velocity profiles were reported in their study.

We present LES results of incompressible, non-reacting flow in a fuel nozzle rig using the method of Mahesh *et al.* (2004). Smagorinsky subgrid-scale model was used together with a slightly modified implementation of the Germano dynamic procedure tailored for unstructured grids. Details on the model implementation and filtering procedure are as in Mahesh *et al.* The geometry is from Pratt and Whitney, and is substantially similar

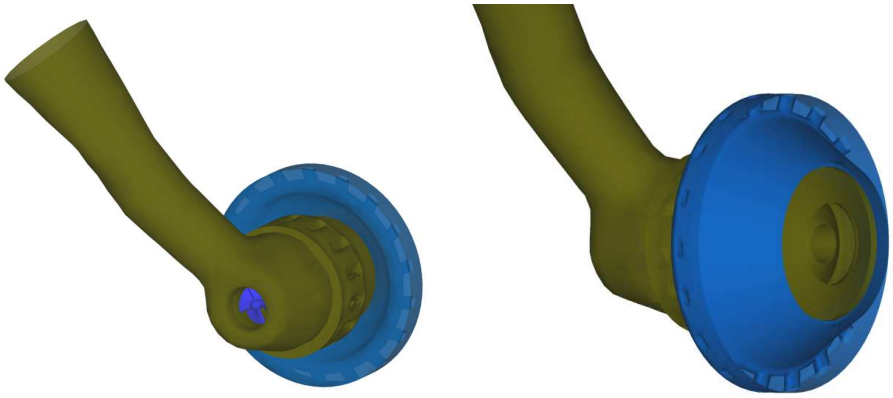

FIGURE 1. Computational model of the Pratt Whitney fuel nozzle rig. Left: side-end view; right: side-front view.

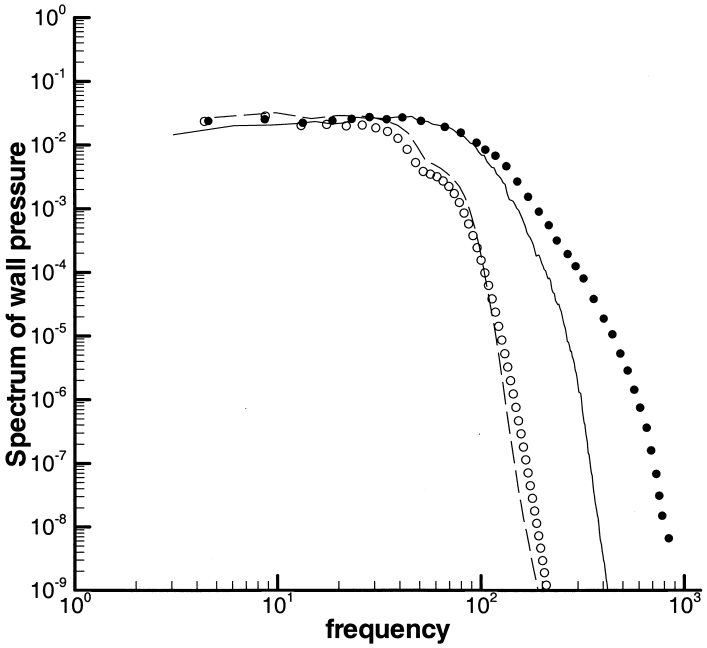

FIGURE 2. Frequency spectrum for wall pressure fluctuations in a planar channel flow. • DNS of Choi & Moin (1990) with a spectral code; ○ coarse LES of Wang with a structured finite difference code (unpublished); solid line: present fine LES; dashed line: present coarse LES.

to that of Brankovic *et al.* (2000) with the exception that the present rig does not have purge holes and their associated intake, see Fig. 1 and the Fig. 1b of Brankovic *et al.* (2000). Validation experimental data for the present nozzle rig flow are also supplied by Pratt and Whitney.

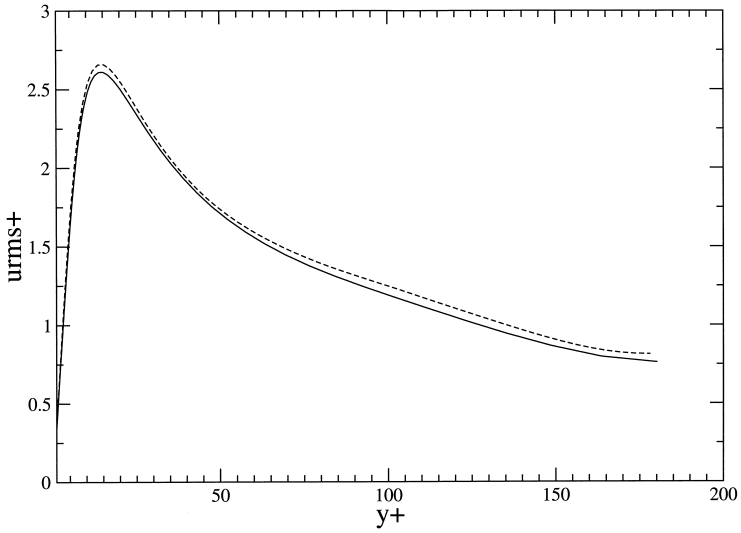

FIGURE 3. Streamwise turbulence intensity in a planar channel flow. Solid line: present fine LES; dashed line: DNS of Moser *et al.* (1999).

2. Validation in simple flows

Prior to computing the flow through injector nozzle, the present unstructured LES computer program (CDP2.1) was first applied to fully developed turbulent planar channel flow for the purpose of validation. Flow conditions and geometrical specifications used in our simulation are identical to those used in the direct numerical simulation (DNS) of Choi & Moin (1990) with a spectral method. In particular, the Reynolds number based on channel half-height and friction velocity is 180. Two mesh sizes were used in the present simulations, (32x64x32) and (128x128x128). The coarse mesh size has a resolution of 72 wall units in the streamwise direction, and 24 wall units in the spanwise direction. These are the same as those used by Meng Wang in a previous channel calculation at the Center for Turbulence Research with a structured second-order finite volume LES code. The fine mesh has the same size as in Choi & Moin. Figure 2 compares the present channel fluctuating wall-pressure spectrum with previous computations. For the calculation of power spectra estimation, a long history of pressure samples was saved at selected locations at every time step. Notations related to power spectrum computation and related post-processing procedures follow strictly those described in Choi & Moin (1990). From Fig. 2 it is clear that at the coarse resolution, our wall pressure spectra results agree well with the results computed previously using a structured LES code by Meng Wang, indicating the reliability of the present code from one perspective. The figure also shows that at the fine resolution our wall pressure spectra agree with the DNS data of Choi & Moin (1990) in the lower frequency range, but there is an earlier drop-off at the high frequency range. This is to be expected because the DNS of Choi & Moin was performed using a spectral code, while the present approach is unstructured second-order finite volume. Figure 3 compares the streamwise turbulence intensity obtained from the

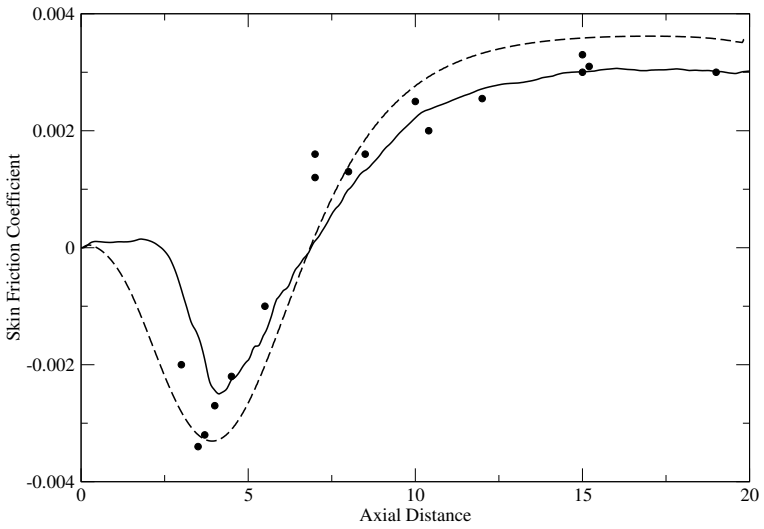

FIGURE 4. Skin friction coefficient in the flow over a backward facing step. • Jovic & Driver (1994); solid line: present LES; dashed line: present RANS.

present LES with that from the DNS of Moser *et al.* (1999). Although not shown here, mean velocity and other second order turbulence statistics from our computation also agree very well with existing DNS channel flow data.

The present computer program was also validated using turbulent flow over a backward-facing step. The flow conditions and geometrical specifications are identical to those reported by Le, Moin & Kim (1997). In particular, the Reynolds number is 5100 based on step height and inlet freestream velocity. The computational domain consists of a streamwise length of 30 step heights, including an inlet section of 10 step heights prior to the sudden expansion, vertical dimension is 6 step heights, and the spanwise width is 4 step heights. Both LES and RANS computations were performed with the same code CDP2.1. For the RANS computation, the V2F turbulence model of Durbin (1995) was implemented into the unstructured LES solver. At the upstream inlet, LES used the zero-pressure gradient flat-plate boundary layer velocity fields obtained from another independent computation. That auxillary computation uses DNS to simulate a spatially developing flat-plate boundary layer through the laminar, transitional and turbulent regimes, covering a range of momentum thickness Reynolds number from 80 to 1000. The boundary layer transitions because of imposed weak, migrating freestream perturbations at the inlet. The time-dependent velocity fields at the station of momentum thickness Reynolds number 700 were saved and subsequently used as inlet conditions for the backward-facing step LES. RANS inflow conditions are from the statistics of Le *et al.*. At the upper boundary, slip wall boundary conditions were applied. Figure 4 compares the predicted skin friction coefficient with the experimental data of Jovic & Driver (1994). The skin friction obtained from the present LES exhibits interesting similarities to the DNS skin friction results of Le *et al.* in the following three respects. Near the step corner, there is region ($0 < x < 2$) with very weak positive skin friction, indicating the existence of a minor secondary recirculation zone. Secondly, the negative peaks attained

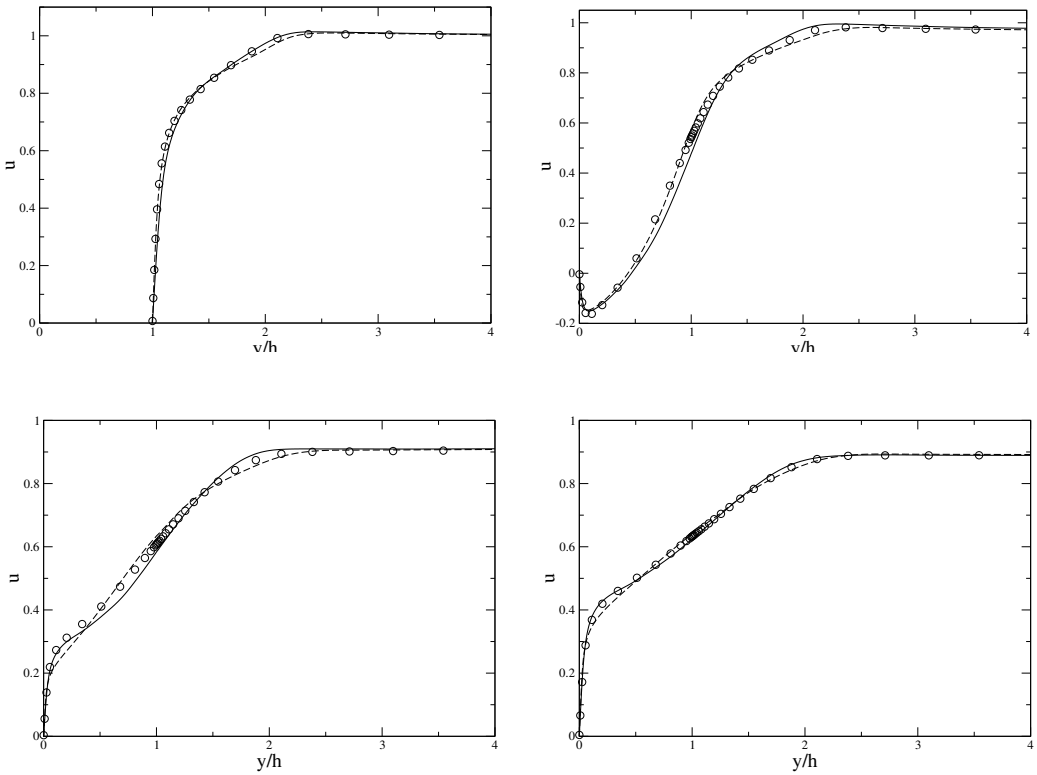

FIGURE 5. Mean streamwise velocity in the flow over a backward facing step. ∘ DNS of Le *et al.* (1997); solid line: present LES; dashed line: present RANS. Upper left: $x = -3$; upper right: $x = 4$; lower left: $x = 10$; lower right: $x = 15$.

in the present LES and in previous DNS are not as deep as that of Jovic & Driver (1994). Further downstream, there is good agreement between the LES and DNS results with the experimental data. Mean streamwise velocity profiles at four different x stations are shown in Fig. 5. Both RANS and LES results show relatively good agreement with the DNS. The minor differences between the RANS and LES velocity profiles are mostly due to the slight discrepancy at the inlet.

3. Results of nozzle rig flow

Figure 1 shows the fuel injector nozzle rig model used in the present LES. Three types of air intakes can be seen from the end view. The central pipe with a small guide vane is the inlet for the core flow. The slots distributed along the circumference with a radius furthermost away from the pipe axis are the tangential entries for guide flow. The slots distributed along the circumference with an intermediate radius (closer to the pipe axis) are the tangential entries for outer flow. From the side-front view, the outlets into the combustor chamber for the core flow, outer flow, and guide flow can be clearly seen. Note the axial position ranges for the three outlets are not the same, i.e., they are staggered. Figure 6 shows cross-sections of the computational domain. The $z = 0$ plane indicates

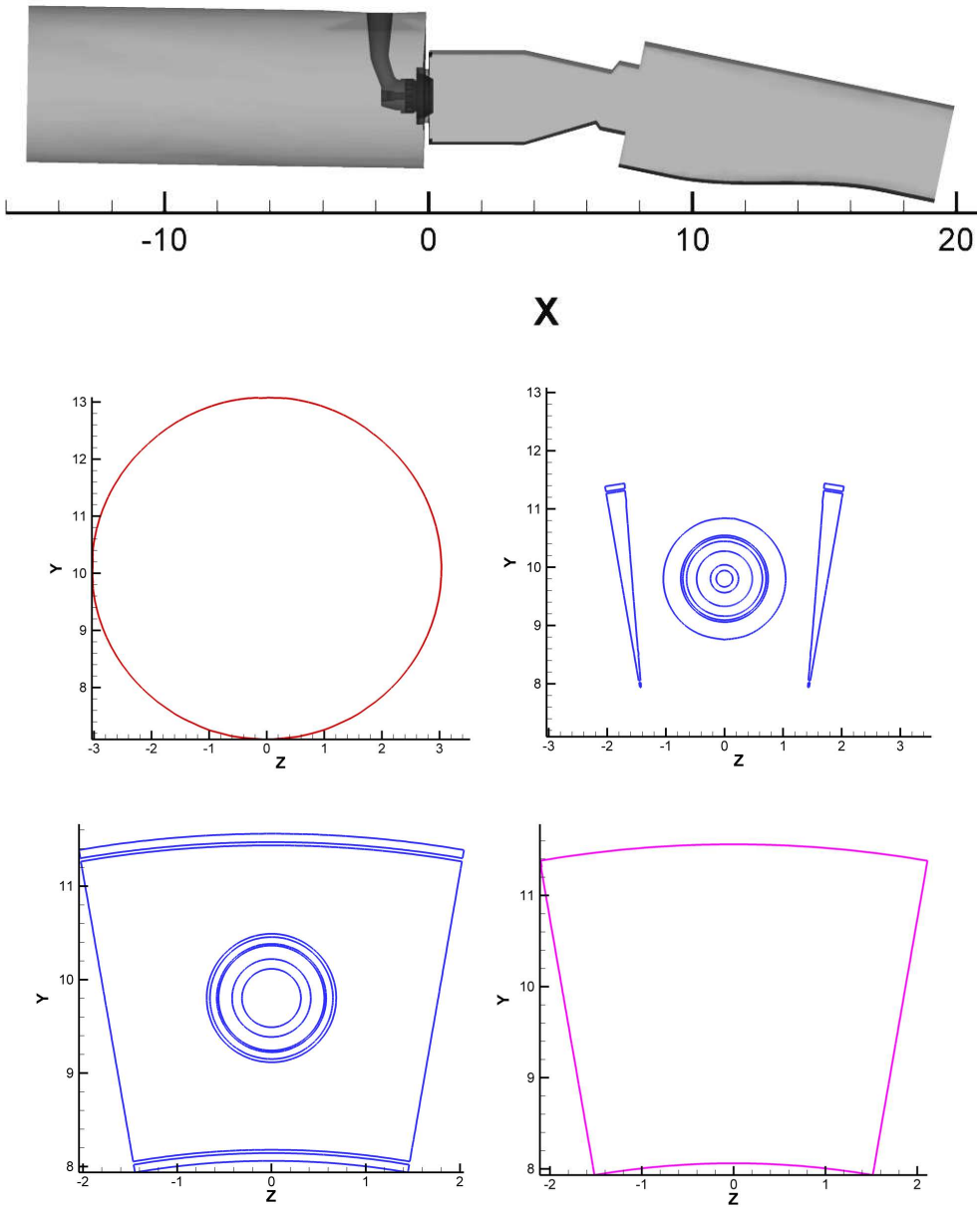

FIGURE 6. Computational domain of the present nozzle rig flow. Upper: $z = 0$ plane; middle left: $x = -4$ plane; middle right: $x = 0$ plane; lower left: $x = 0.01$ plane; lower right: $x = 2$ plane.

that axial coordinate x covers a range of $-15.5 < x < 20$, approximately. At $x = -4$, the cross-section of the computational domain is a full 360° circular pipe. Downstream of the nozzle at $x = 2$, the cross-section becomes a circular sector. As indicated in the figure, the nozzle axis is located at $y = 9.8$ and $z = 0$.

At the far upstream uniform inlet velocity was prescribed as 29.134 in/sec using ex-

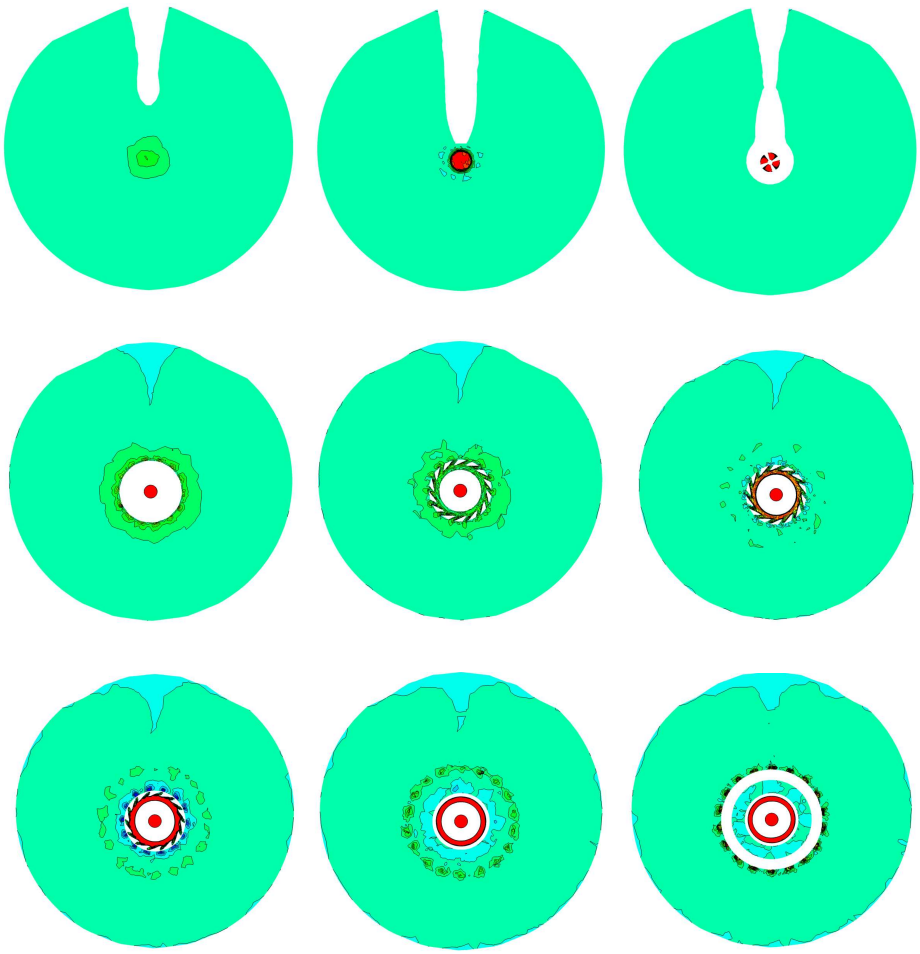

FIGURE 7. Contours of instantaneous axial velocity inside nozzle, light colors represent low axial speed. From top left to lower right (row major) the locations for the cross-sections are: $x = -2.1$, -1.8, -1.55, -0.9, -0.8, -0.7, -0.6, -0.5, -0.45, respectively.

perimental specifications. The Reynolds number based on inflow speed and unit length (1 inch) is 1246. Except for the inlet and outlet all the other boundary surfaces of the geometry are solid wall on which no-slip conditions were applied. A total of six calculations were performed with mesh sizes ranging from 3.6 to 8 million cells; they yielded similar and consistent results. Mesh shape and density in the region close to nozzle outlet were varied in the six cases. The maximum CFL number was set at 4.5 and the corresponding time step is approximately 7.0×10^{-7} seconds. It was found that 2×10^5 time steps are needed to converge the mean flow statistics.

The process of swirl generation by nozzle injector is complicated and can be appreciated by examining the velocity fields over a series of cross-sections perpendicular to the x-direction. Figure 7 shows the axial velocity contours over nine yz-planes up to $x = -0.45$. White space in the first three planes represents slices of the fuel stem hardware. The high-speed contours near the pipe axis in the plane of $x = -1.8$ is the core flow. The four small fan-like structures at $x = -1.55$ are due to the effect of guide vane inside the core

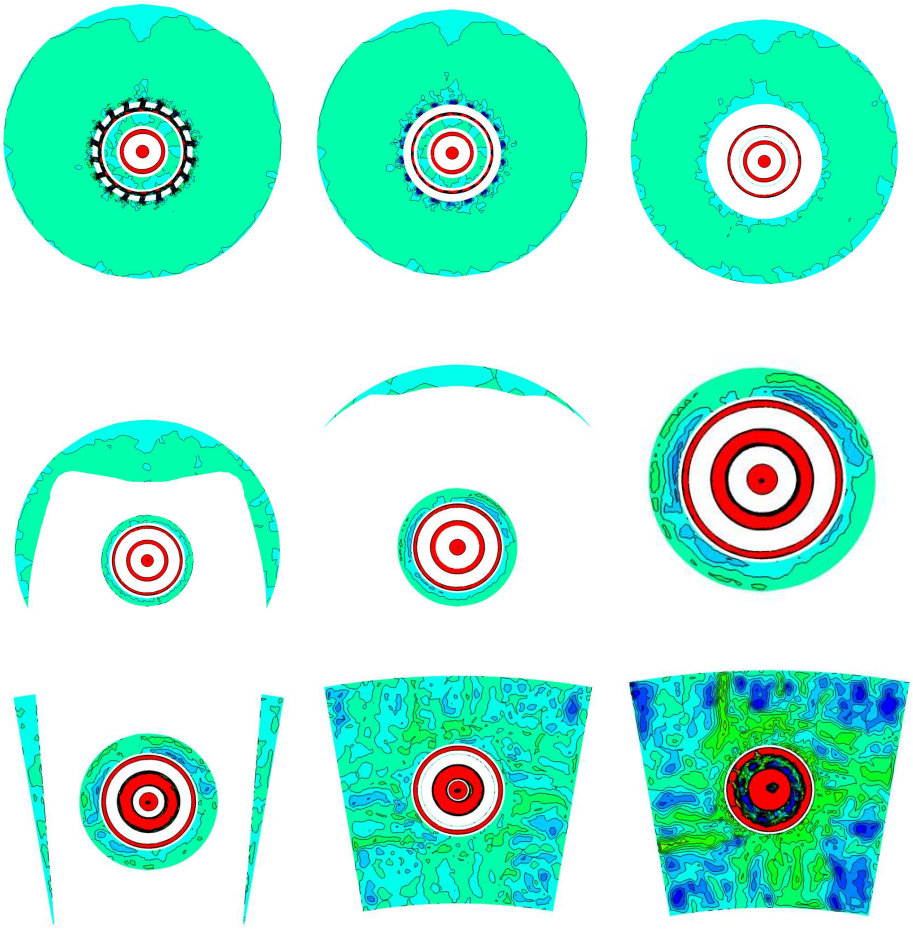

FIGURE 8. Contours of instantaneous axial velocity inside nozzle, light colors represent low axial speed. From top left to lower right (row major) the locations for the cross-sections are: $x = -0.4$, -0.35, -0.20, -0.15, -0.10, -0.05, 0.00, 0.05, 0.15, respectively.

flow intake. The tangential outer flow intakes are clearly visible on the three planes of $x = -0.8$, -0.7 and -0.6. Also visible over these planes is the velocity wake behind the fuel stem. At the last two cross-sections the guide flow entries start to affect the flow, as indicated by the sparsely connected outer ring-like structures in the velocity contours. The actual guide flow entry slots are shown in the cross-section of $x = -0.4$ in Fig. 8. Over the yz-plane of $x = -0.2$ there are four isolated flow streams: core stream, outer stream, guide stream as well as the flow occupying the reminder of the container pipe. At the station of $x = -0.1$ the upstream container pipe has nearly ended, see also Fig. 6. Therefore almost all the inlet fluid mass now squeezes through the narrow passages near the nozzle axis. These ring-like flow streams merge further downstream inside the combustion chamber. Unlike the upstream pipe which covers a full 360° range, the downstream combustor spans only a small angular section, see the yz-plane of $x = 0.05$ and 0.15.

Convergence of numerical solutions in complex swirling flows is more difficult than in the two simple canonical flows used for the validation study. We found that the mean

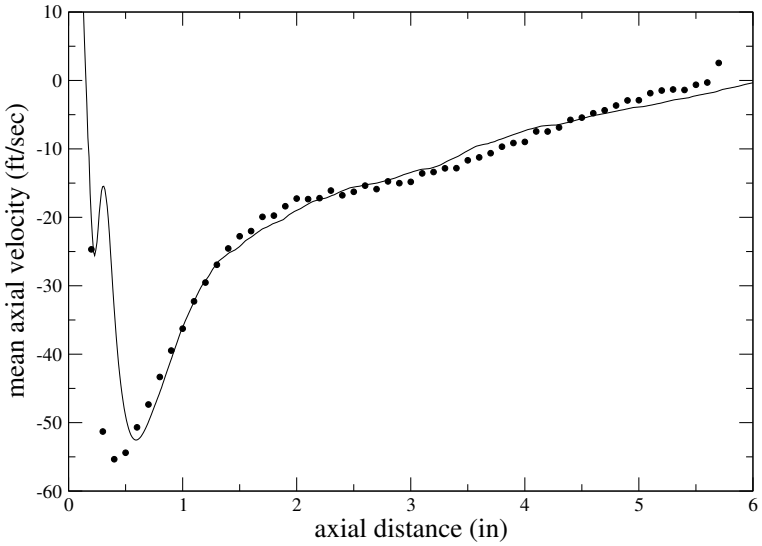

FIGURE 9. Mean axial velocity along the injector geometric centerline. • Pratt Whitney experiment; solid line: present LES.

centerline axial velocity can be used as a good indicator for monitoring convergence of LES solutions in the present nozzle rig swirling flow. For example, when a new simulation is initiated by interpolating converged solutions from an existing case with different mesh shape or mesh density, it takes another 2×10^5 time steps for the mean centerline axial velocity to reach statistically steady state. The predicted mean axial velocity along the injector geometric centerline in Fig. 9 is seen to agree with the Pratt Whitney experimental data over a significant portion of the axial distance with the exception of $0.2 < x < 0.6$. The present comparison represents a substantial improvement from that shown in the Fig. 12 of Brankovic *et al.* (2000). Note the geometries in these two studies are slightly different and the current experimental data set is close but not the same as those in Brankovic *et al.* The predicted secondary negative peak of mean axial velocity at $x \approx 0.2$ was found to be very persistent through a series of test simulations with significant changes in mesh density and composition (tetrahedral versus textural), especially in the region immediately downstream of the $x = 0$ plane. Inspection of the instantaneous and mean velocity contours over the symmetry plane of $y = 9.8$ reveals a tiny region centered at approximately $x = 0.2$ with slightly stronger negative flow compared to the region immediately downstream from $0.2 < x < 0.3$. Beyond $x = 0.3$ is the main central recirculation zone where the primary negative peak is located. The tiny patch centered at $x = 0.2$ likely arises from the interaction between the core swirling flow and the outer swirling flow, and the main central recirculation zone is due to the combined effects of all the three swirling streams. Mixing between the core and outer swirling streams occurs upstream of the guide flow outlet. Recall that the three outlets are staggered in axial position ranges. The calculated mean axial and radial velocities over the symmetry plane $y = 9.8$ as a function of distance from the injector centerline are compared with experimental data in Fig. 10. The comparison is overall satisfactory.

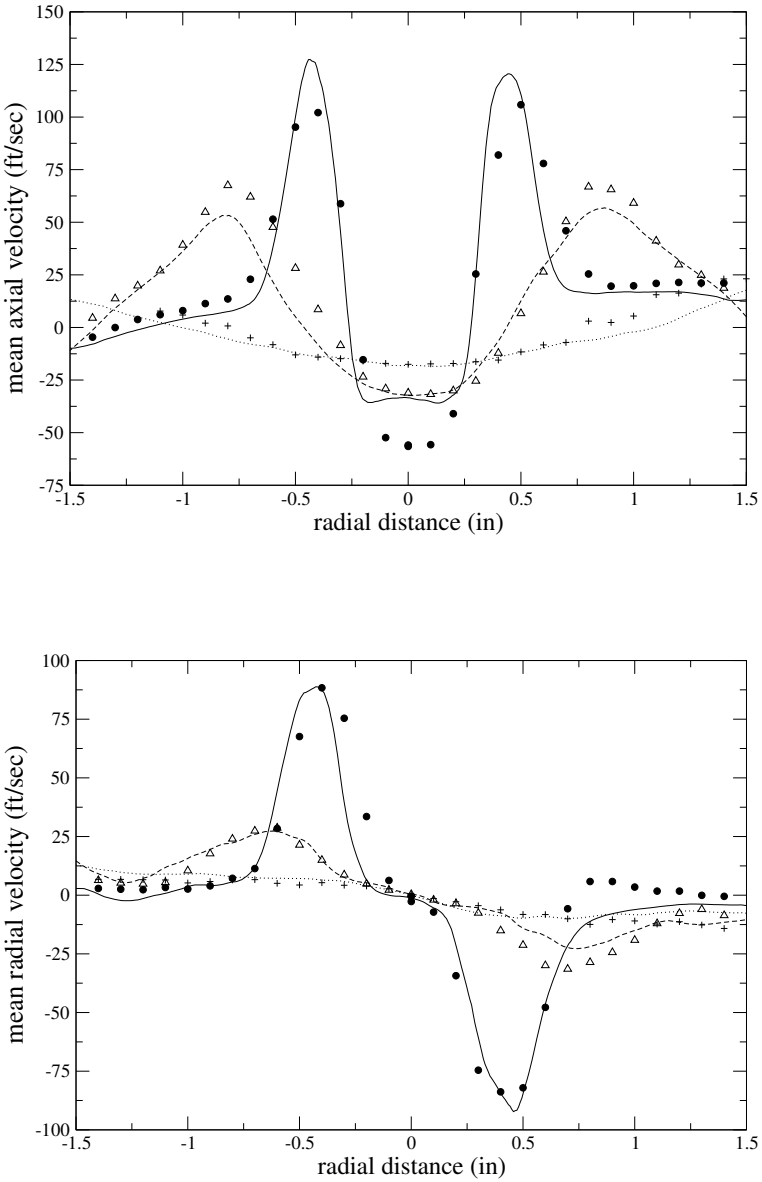

FIGURE 10. Mean velocities as a function of radial distance over the symmetry plane of $y = 9.8$. Upper: axial velocity; lower: radial velocity. • solid line $x = 0.4$; △ dashed line $x = 1.1$; + dotted line $x = 2.1$. Symbols are experimental data and lines are present LES.

The underprediction of the primary negative peak at $x = 0.4$ is directly related to the discrepancy shown in Fig. 9. Swirling vortex is generated near the nozzle as a result of the interaction of the three jet streams. This is visualized in Fig. 11 using surfaces of

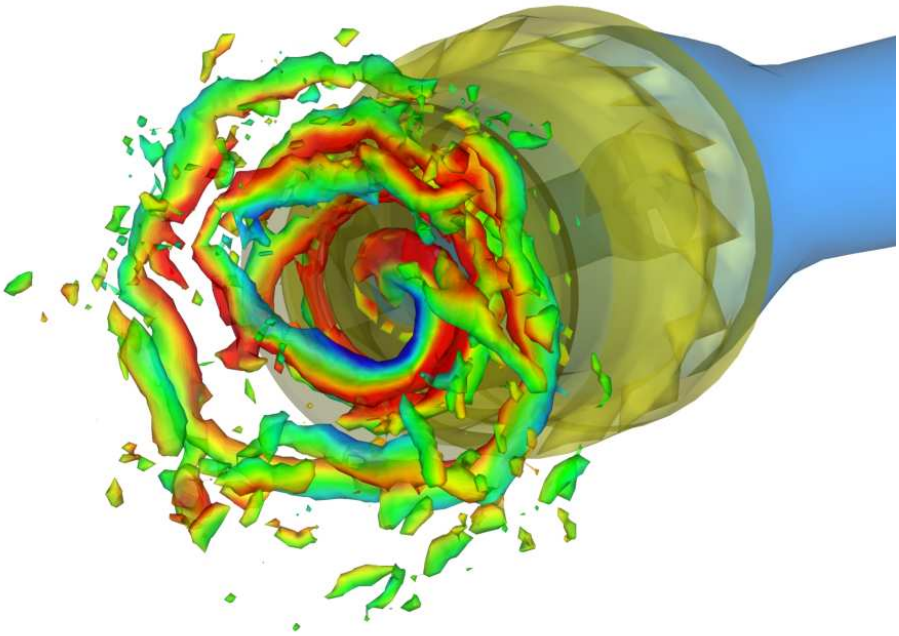

FIGURE 11. Visualization of swirling vortex near the injector using the second-invariant of the velocity gradient tensor.

the second invariant of the velocity gradient tensor. The darkened region in the figure represents higher axial speed.

4. Conclusions

Inclusion of the swirl-generating device geometry is an integral part of jet engine combustor fluid flow simulation. In this work we have applied an unstructured, energy-conserving LES approach to the computation of non-reacting flow in a realistic fuel injector nozzle. Validation results obtained for channel and backward facing step flows are in good agreement with existing DNS and experimental data. LES results for the complex nozzle rig flow demonstrated marked improvement over previous RANS results with respect to comparison with experimental measurements. The effects of the injector nozzle components are revealed through visualization of the velocity fields over a sequence of cross-sections perpendicular to the nozzle axis. Additionally, the axial velocity along the injector centerline was found to be a good indicator of solution convergence in the present swirling flow. When a new simulation is initiated using interpolated solutions from an existing converged case with different mesh shape or density, it takes nearly the same number of time steps to converge the new solution as required in the original simulation with zero initial velocity field.

Acknowledgments

Discussions with Sourabh Apte, George Constantinescu, Krishnan Mahesh, Cliff Wall, and Meng Wang are acknowledged. This work is supported by the Advanced Simulation

and Computing program of the United States Department of Energy. We are thankful to Pratt and Whitney for kindly supplying the fuel nozzle rig geometry and validation experimental data. The simulations were performed on the IBM terascale parallel machine at the San Diego Supercomputing Center.

REFERENCES

Brankovic, A., McKinney, R., Quyang, H., Porter, L., Kennedy, J., Madabhushi, R. & Colket, M. 2000, Comparison of measurements and predictions of flow in a gas turbine engine fuel nozzle. *AIAA Paper 2000-0331.*

Choi, H. & Moin, P. 1990, On the space-time characteristics of wall-pressure fluctuations. *Phys. Fluids*, **2**, 1450-1460.

Durbin, P.A. 1995, Separated flow computations with the $k-\epsilon-v^2$ model. *AIAA J.* **33**, 659-664.

Grinstein, F.F., Young, T.R., Gutmark, E.J., Li, G., Hsiao, G. & Mongia, H.C. 2002, Flow dynamics in a swirl combustor. *J. Turbulence* **3**, article 30.

Jovic, S. & Driver, D.M. 1995, Reynolds number effects on the skin friction in separated flows behind a backward facing step. *Exps. Fluids* **18**, 464-467.

Le, H., Moin, P. & Kim, J. 1997, Direct numerical simulation of turbulent flow over a backward-facing step. *J. Fluid Mech.*, **330**, 349-374.

Mahesh, K., Constantinescu, G. & Moin, P. 2004, A numerical method for large eddy simulation in complex geometries. *J. Comp. Phys.* **197**, 215–240.

Moser, R.D., Kim, J. & Mansour, M.N. 1999, DNS of turbulent channel flow up to $Re_\tau = 590$. *Phys. Fluids*, **11**, 943-945.

Pierce, C.D. & Moin, P. 1998, Method for generating equilibrium swirling inflow conditions. *AIAA J.*, **36**, 1325-1327.

Roux, S., Lartigue, G., Poinsot, T., Meier, U. & Berat, C. 2005, Studies of mean and unsteady flow in a swirled combustor using experiments, acoustic analysis and large eddy simulations. *Combust. Flame*, **141**, 40-54.